



Hydrogen production by reforming of acetic acid using La–Ni type perovskites partially substituted with Sm and Pr

K.A. Resende^a, C.N. Ávila-Neto^a, R.C. Rabelo-Neto^b, F.B. Noronha^b, C.E. Hori^{a,*}

^a Federal University of Uberlândia, School of Chemical Engineering, Av. João Naves de Ávila, 2121, Bloco 1 K, 38408-144, Uberlândia, MG, Brazil

^b National Institute of Technology, Division of Catalysis and Chemical Processes, Av. Venezuela, 82, Centro, 20081-312 Rio de Janeiro, RJ, Brazil



ARTICLE INFO

Article history:

Available online 22 August 2014

Keywords:

Bio-oil aqueous fraction
Perovskite
Nickel
Acetic acid and hydrogen

ABSTRACT

The condensation of gases from the pyrolysis of biomass leads to a liquid compound called bio-oil. This oil can be divided into two fractions: one aqueous and another non-aqueous. The aqueous fraction does not have a high market value and it is usually discarded. However, this mixture has considerable amounts of organic compounds, which can be potential renewable sources of hydrogen. Steam reforming has been the most studied reaction to produce hydrogen from the aqueous fraction of bio-oil. Due to the diversity of organic compounds found in this aqueous fraction, model compounds have usually been used to study this mixture. Among the compounds used to represent the aqueous fraction of bio-oil, acetic acid is the most popular. Nickel-based catalysts are traditionally used for reforming reactions. An alternative to combine high Ni content employed in catalysts, this kind of process with desirable values of dispersion is to use perovskite-type precursors (LaNiO_3). Therefore, the objective of this study was to investigate the production of hydrogen from the aqueous fraction of bio-oil. More specifically, in this work, LaNiO_3 , LaPrNiO_3 and LaSmNiO_3 were tested as precursors for catalysts in the reaction of steam and oxidative reforming of acetic acid. During the reaction, the catalysts showed the formation of the same products: H_2 , CO , CH_4 , CO_2 , $\text{C}_3\text{H}_6\text{O}$, but with different selectivities. All samples presented good selectivity for hydrogen formation, and the presence of Pr and Sm just slightly affected the catalytic performance. Due to the large accumulations of coke observed during the reaction of steam reforming, a small amount of O_2 was added to the mixture. The presence of this oxidant improved catalytic activity without reducing the amount of hydrogen produced. Furthermore, it helped to reduce the deposits of coke, maintaining the catalytic activity during 24 h of reaction.

© 2014 Elsevier B.V. All rights reserved.

1. Introduction

Hydrogen is an important alternative for energy generation and it presents several advantages, such as a high specific energy ($\sim 120 \text{ MJ kg}^{-1}$), formation of water as the only product during the combustion process, among others [1]. Nowadays, hydrogen production occurs mainly through reforming of natural gas. However, the goal of sustainable development requires the use of renewable sources, such as biomass or water electrolysis [2]. Biomass is the renewable energy source with greater availability worldwide and it has a high-energy potential. According to Huber and Dumesic [3], it is important to develop technologies that will make the use of biomass economically viable. Gasification and pyrolysis are the most used processes for the energetic use of biomass [4].

Pyrolysis consists on a thermal decomposition of biomass in the absence of oxygen or water vapor [5]. During this process, a dark colored liquid called bio-oil is formed. It is a complex mixture with different types of organic compounds, such as carboxylic acids, ketones, aldehydes, sugars, alcohols, phenols, water and more complex compounds [6,7]. When water is added to bio-oil, it separates into two fractions. One of the fractions is non-aqueous and contains lignin derivatives. This fraction has characteristics similar to oils obtained from fossil fuels, which gives it a high economic value [8]. The other fraction is aqueous and contains acids, ketones, aldehydes and others compounds in low concentrations. Therefore, this aqueous phase does not have many applications and it is discarded in most cases. The catalytic reforming of the aqueous fraction of bio-oil to obtain hydrogen could be an interesting way to increase the production and use of bio-oil [9]. According to Yan et al. [10], this strategy has low costs and it is trouble-free. The aqueous fraction of bio-oil usually has around 80 wt% of water, which could feed the demand for water in the steam reforming process.

* Corresponding author. Tel.: +55 34 3239 4292; fax: +55 34 3239 4249.

E-mail addresses: cehori@ufu.br, cehori@gmail.com (C.E. Hori).

Steam reforming is the most reported reaction used to produce H₂ from the aqueous fraction of bio-oil [11]. Many studies report the production of H₂ from steam reforming of the aqueous fraction extracted from different types of bio-oils [10,12,13]. Acetic acid is the most abundant organic compound in the aqueous fraction of various types of bio-oil [14], and because of this, it is usually reported as a representative molecule of this fraction. However, other model molecules such as acetol [15], ethylene glycol [16], acetone [17], among others [18], are also studied.

The major problem of steam reforming of the aqueous fraction of the bio-oil is the formation of large amounts of coke, which deposits on the catalyst surface. This accumulation contributes to the deactivation of the catalyst and it also causes a decrease in H₂ selectivity [19–23]. According to Hu and Lu [24], Ni has a significant catalytic activity for this reaction and it is economically feasible [16,25].

Fatsikostas et al. [27] showed that Ni-based catalysts (17 wt%) supported on La₂O₃ exhibited high activity and selectivity to hydrogen formation in steam reforming of ethanol. According to the authors, the presence of La improved the catalyst performance. When the catalyst promoted with La is subjected to reducing conditions, this metal forms a thin LaO_x layer on the surface of Ni particles. This layer can react with CO₂ to form lanthanum oxy-carbonate (La₂O₂CO₃), which combines with the deposited carbon and cleans the Ni surface. The concentration of the active metal also affects the rate of carbon accumulation. Li et al. [22] tested Ni-based catalysts supported on ZrO₂ with Ni content varying from 0 to 23% in steam reforming of acetic acid. They noticed an appreciable increase in Ni particle size for higher concentrations of Ni, which affected its dispersion. Furthermore, it was also shown that the presence of large Ni crystallites promotes the formation of carbon [22,28]. Thus, the balance between the rates of formation and oxidation of carbon deposits may be achieved by decreasing the size of metal crystallites.

One way to combine both high loadings of Ni and high dispersion is to obtain a catalyst from a method known as solid-phase crystallization [29]. In this method, the active phase (Ni) is extracted from a well-defined solid structure when it is submitted to a treatment in a reducing atmosphere. Perovskites (ABO₃) are examples of solid structures used for this purpose [30–34]. In addition, they have the ability to allow the substitution of cations in both positions A and B by other similar sizes elements, A' and B', which can lead to better catalytic properties. Gallego et al. [35] studied the use of perovskites La_{1-x}A_xNiO_{3-δ} (A = Pr and Ce, x = 0–0.06) as precursors of active catalysts for dry reforming of methane. The authors observed that the addition of Ce and Pr to the perovskite-type structure, LaNiO₃, decreased the Ni crystallite size. It also contributed to improve the performance of the samples during the reaction. It was shown that the rate of carbon accumulation on the catalyst surface decreased as the amount of dopant (Ce and Pr) increased. These observations were probably due to two factors: (i) the particle size of metallic Ni present in the doped catalysts decreased and (ii) Ce and Pr have redox properties. Jahangiri et al. [36] also studied a series of perovskite precursors doped with Sm (La_{1-x}Sm_xNiO₃, x = 0–1). The results showed that the preparation method led to the formation of a homogeneous and crystalline structure with a small amount of Sm. The high activity of the catalyst doped with high amounts of Sm was justified by its catalytic redox properties.

In order to improve the technology of obtaining H₂ from biomass, the objective of this work is to study the production of H₂ from the aqueous fraction of bio-oil through reforming processes using Ni-based catalysts. Activity and stability tests during steam (SR) and oxidative reforming of acetic acid (OSR) were conducted using catalysts derived from a La–Ni perovskite-type structure doped with Pr and Sm.

2. Experimental

2.1. Catalyst preparation

The perovskite precursors were synthesized by a precipitation method adapted from de Lima et al. [37]. The first sample, named LaNiO₃, was prepared with equimolar amounts of Ni and La (Ni/La = 1). In the two other samples, La atoms were partially replaced by Pr or Sm. These samples are named LaPrNiO₃ and LaSmNiO₃, where 0.1 is the fraction of replaced La atoms. To prepare the LaNiO₃ precursor, an aqueous solution of Na₂CO₃ (0.5 M) was added rapidly and under vigorous stirring to a freshly prepared aqueous solution of La(NO₃)₃·6H₂O and Ni(NO₃)₂·6H₂O until reaching pH 8. In the case of the LaPrNiO₃ and LaSmNiO₃ precursors, stoichiometric amounts of Pr(NO₃)₂·6H₂O and Sm(NO₃)₃·6H₂O salts were also added to the above solution. Following, the precipitate was washed and filtered under vacuum for removing remaining contaminant ions. The washed solid was then dried in a furnace at 338 K for 20 h and calcined under flow of synthetic air (50 mL min⁻¹) in two stages: first at 723 K (heating rate of 1.5 K min⁻¹) for 4 h and finally at 1173 K (heating rate of 5 K min⁻¹) for 6 h.

2.2. Characterization

X-ray powder diffraction (XRD) analyses were carried out (i) in conventional mode at room temperature and (ii) during in situ heating of the samples under a flow of H₂ in He (5 vol%).

In conventional mode, XRD patterns of the calcined and reduced/passivated samples were obtained with a Rigaku equipment, using Cu K α radiation (1.54056 Å) with a Ni filter. The 2 θ angle was swept from 10° to 80°, with a step size of 0.02° and a counting time of 2 s per step. The Scherrer equation was used to estimate the crystallite mean diameter of NiO and Ni⁰ particles. For the measurements of the crystallite mean diameter of metallic Ni particles, the calcined samples were also reduced under pure hydrogen (30 mL min⁻¹) at 773 K for 1 h, purged under N₂ at the same temperature for 30 min and cooled to 298 K. Then, the reactor was maintained at 203 K for 1 h, the catalyst was passivated with a 5% O₂/N₂ mixture.

In situ XRD was carried out at the XPD-10B beamline of the Brazilian Synchrotron Light Laboratory (LNLS). The samples were first crushed, sieved to particle sizes smaller than 20 μ m and homogeneously distributed over the support. XRD patterns were then acquired during heating of the samples from room temperature to 973 K, at 5 K min⁻¹, with a holding time of 30 min, under a 200 mL min⁻¹ flow of H₂/He (5 vol%). Scans were carried out from 20° to 55°, with a step size of 0.003° and a counting time of 1 s, using a wavelength of 1.65121 Å and a resolution of 4.3 eV.

Temperature-programmed reduction (TPR) measurements were conducted using a quadrupole mass spectrometer (OmniStar-Balzers). The samples (50 mg) were reduced under a 2% H₂/Ar mixture (30 mL min⁻¹) at a heating rate of 10 K min⁻¹ from 298 to 1273 K.

Temperature-programmed desorption (TPD) of acetic acid experiments were performed in the same apparatus previously described for TPR. In a typical TPD experiment, 100 mg of the catalyst was reduced under pure H₂ (30 mL min⁻¹) at a heating rate of 10 K min⁻¹ up to 973 K for 2 h. After activation, the H₂ flow was shifted to Ar flow (30 mL min⁻¹) and the samples were cooled to room temperature. Adsorption of acetic acid was carried out at 390 K for 30 min by flowing argon (30 mL min⁻¹) through a saturator filled with acetic acid kept at 293 K. Then the sample was purged with Ar flow for 30 min, and the temperature was linearly increased with a heating rate of 10 K min⁻¹ up to 1023 K.

The effluent composition was monitored by a quadrupole mass spectrometer (OmniStarBalzers).

Thermogravimetric analysis of the used catalysts was carried out in a TA Instruments equipment (SDT Q600) in order to determine the amount of carbon formed over the catalyst. Approximately 12 mg of spent catalyst was heated under air flow from room temperature to 1273 K at a heating rate of 20 K min⁻¹ while the weight change was measured. Other characterizations of the used catalyst were not performed due to the small mass available.

2.3. Activity tests

Prior to the reactions, samples (10 mg of catalyst diluted with 150 mg of SiC) were reduced under pure hydrogen flow (30 mL min⁻¹) at 973 K for 1 h. Steam reforming (SR) of acetic acid was carried out in a fixed-bed tubular reactor (Hastelloy X) at 873 K and atmospheric pressure using a Microactivity Reference equipment (PID Eng & Tech.). The reactant mixture (water/acetic acid molar ratio of 3) was injected with a piston pump (Gilson) and vaporized in a He stream. The composition of the reactant mixture was 13% acetic acid, 39% water, 48% helium, with the total flow rate of 400 mL min⁻¹. The reaction products were analyzed online by gas chromatography (Agilent 7890A) equipped with a thermal conductivity detector (TCD) detector and a Porapak Q column.

Oxidative steam reforming (OSR) of acetic acid was performed in a fixed-bed quartz reactor at 873 K and atmospheric pressure. The water and acetic acid were fed using two parallel saturators with Ar streams (100 mL min⁻¹ each). The saturated streams were mixed with O₂ stream (5 mL min⁻¹ each). The total feed consisted of a 205 mL min⁻¹ stream with 11% acetic acid, 13% steam, 2% O₂ and 74% Ar. The effluent was analyzed by online gas chromatography employing a Shimadzu gas chromatograph equipped with a thermal conductivity detector (TCD), a flame ionization detector (FID) and two columns: Carboxen 1010 Plot and Rtx®-5.

The molar fraction in dry basis of species *i* (y_i) and the conversion of acetic acid (X_{Ac}) for both steam reforming and oxidative reforming were calculated by Eqs. (1) and (2), respectively.

$$y_i (\%) = \frac{F_i}{\sum_{j=1}^N F_j} \times 100 \quad (1)$$

$$X_{Ac} (\%) = \frac{F_{Ac,in} - F_{Ac}}{F_{Ac,in}} \times 100 \quad (2)$$

In Eqs. (1) and (2), F_i and F_j are the molar flows of species *i* and *j* in the reactor outlet stream (H₂, CH₄, CO, CO₂ and acetone), respectively, and $F_{Ac,in}$ is the molar flow of acetic acid in the inlet stream.

3. Results

3.1. Catalyst characterization

Fig. 1A shows the XRD patterns of the calcined samples. All samples show diffraction lines around 23.35°, 47.27° and 58.64°. These lines correspond to the lattice planes of LaNiO₃, where Ni atoms have valence 3+, indicating that the calcination conditions were sufficient to form the perovskite-type structure [33,38]. The samples also show a triple line around 32.3°, 32.8° and 33°, which may be attributed to another perovskite-type phase, the La₄Ni₃O₁₀. In this type of structure, the Ni valence is close to 2.67+. Diffraction lines around 37.3°, 43.3° and 63.1° were also identified and may be attributed to lattice planes (111), (200) and (220) of NiO. Since the syntheses were performed with equimolar amounts of Ni and La, the former results indicate that a small amount of Ni did not enter the perovskite-type structure. Diffraction lines corresponding to praseodymium or samarium oxides were not identified, which

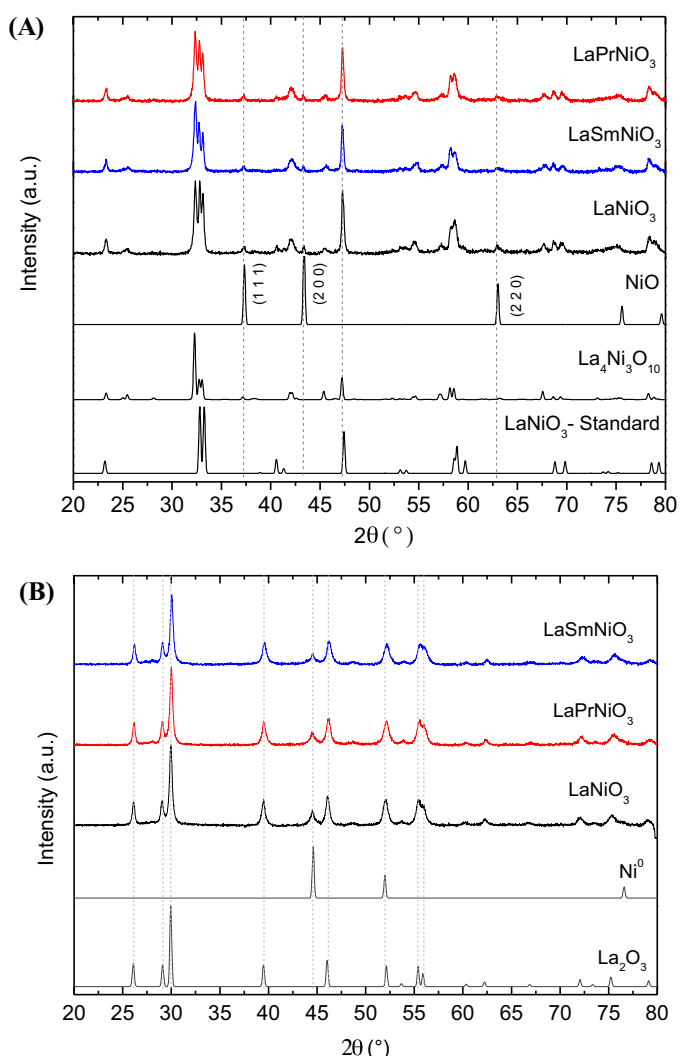


Fig. 1. XRD patterns of (A) calcined and (B) reduced and passivated LaNiO₃, LaPrNiO₃ and LaSmNiO₃ samples. XRD patterns of NiO, La₄Ni₃O₁₀, LaNiO₃, Ni⁰ and La₂O₃ taken from the Inorganic Crystal Structure Database (collection codes 24014, 80279, 67714, 43397 and 24693, respectively).

indicates that these metals were incorporated in the perovskite-type structure, at least partially. Similar results were reported in the literature [35,36]. The three samples exhibit similar average crystallite sizes, with values close to 20 nm. This value agrees with previous results [39] and shows that the addition of Pr and Sm do not alter significantly the average crystallite sizes of the precursors.

XRD patterns of the reduced and passivated samples are displayed in **Fig. 1B**. The diffractograms revealed the presence of lines corresponding to La₂O₃ (26.1°, 29.1°, 29.9°, 39.64°, 46°, 52°, 55.6° and 56.1°) and Ni⁰ (44.5° and 52°) phases. These results indicate that both perovskite-type structures, LaNiO₃ and La₄Ni₃O₁₀, were destroyed during the reduction treatment, giving rise to Ni⁰ particles deposited over lanthanum oxide. **Table 1** shows the size of Ni⁰ crystallites estimated by applying the Scherrer equation. The addition of Pr and Sm to the LaNiO₃ perovskite-type structure caused a slight decrease in the size of Ni⁰ crystallites from 21 nm (LaNiO₃) to 18 nm (LaPrNiO₃ and LaSmNiO₃) [35,40–44].

Fig. 2 shows the temperature-resolved XRD patterns obtained for the calcined LaNiO₃ sample heated in a H₂/He mixture (5 vol%). At 473 K, the diffractograms reveal the presence of lines corresponding to LaNiO₃ (23.35° and 47.27°), La₄Ni₃O₁₀ (32.3°) and NiO (37.3° and 43.3°), which were also observed in **Fig. 1A**. Between

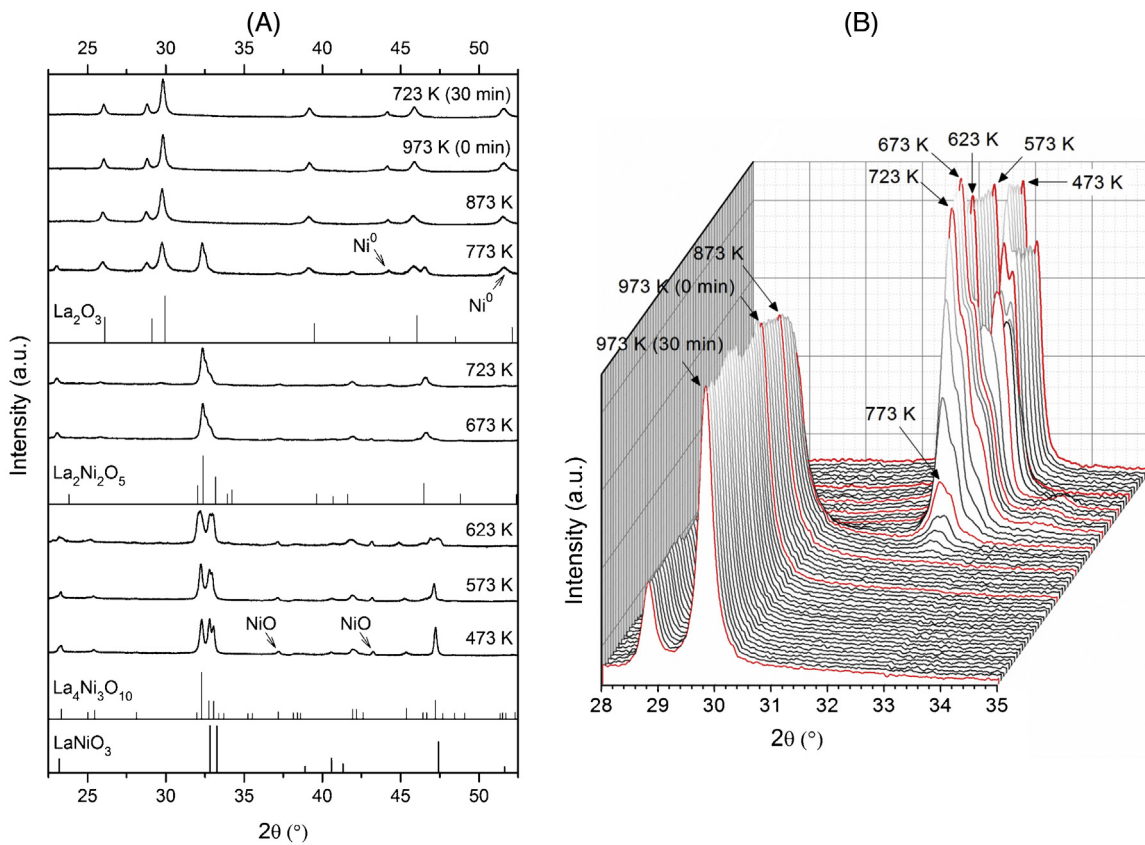


Fig. 2. Temperature-resolved XRD patterns in (A) two dimensions (2D) with $2\theta = 20\text{--}55^\circ$ and in (B) three dimensions (3D) with $2\theta = 28\text{--}35^\circ$. Heating rate: 5 K min^{-1} ; carrier flow: H_2/He (5 vol%). XRD patterns of NiO , $\text{La}_4\text{Ni}_3\text{O}_{10}$, LaNiO_3 , Ni^0 , La_2O_3 taken from the Inorganic Crystal Structure Database (collection codes 24014, 80279, 67714, 1917 and 24693, respectively) and $\text{La}_2\text{Ni}_2\text{O}_5$ taken from Crespin et al. [45].

473 and 623 K, the structures seem to reorganize and lose crystallinity. The gradual increase in the width at half height of the lines around 32.3° , 32.8° , 33° and 47.27° illustrates this fact. According to Crespin et al. [44,45], the calcined sample suffers a deviation from the oxygen stoichiometry when it is heated, which causes a disorder in the perovskite-type structure. A third perovskite phase ($\text{La}_2\text{Ni}_2\text{O}_5$), with lines around 32.36° and 46.48° , appears at 673 K and seems to be stable until 723 K. For higher temperatures, the $\text{La}_2\text{Ni}_2\text{O}_5$ perovskite-type structure is destroyed and gives rise to Ni^0 particles deposited over lanthanum oxide, as already shown in Fig. 1B. Indeed, La_2O_3 (26.1° , 29.1° , 29.9° , 39.64° , 46° and 52°) and Ni^0 (44.5° and 52°) are the unique phases observed for temperatures higher than 873 K. This is an evidence that the perovskite-type structure $\text{La}_4\text{Ni}_3\text{O}_{10}$ follows the same reduction mechanism of LaNiO_3 .

Fig. 3 presents the TPR profiles of LaNiO_3 , LaPrNiO_3 and LaSmNiO_3 samples. The reduction profile of all perovskite-type oxides exhibited two peaks at $689\text{--}702\text{ K}$ and $860\text{--}913\text{ K}$. These peaks are shifted to higher temperatures if compared to those reported in the literature [31,40] and to those observed in the in situ XRD analysis. This is likely due to the lower hydrogen concentration

used in this study (2% H_2/N_2). According to the literature [37,40], the reduction peak at low temperature is assigned to the reduction of Ni^{3+} to Ni^{2+} . Indeed, Fig. 2A shows that the reduction of Ni^{3+} to Ni^{2+} starts around $600\text{--}700\text{ K}$, which was also observed by Rivas et al. [44]. The transition of LaNiO_3 to $\text{La}_2\text{Ni}_2\text{O}_5$ also occurred in this temperature range (see Eq. (3) [44,45]). The peak at high temperature is attributed to the reduction of Ni^{2+} to Ni^0 according to Eq. (4) [29], which is also in agreement with the in situ XRD data.

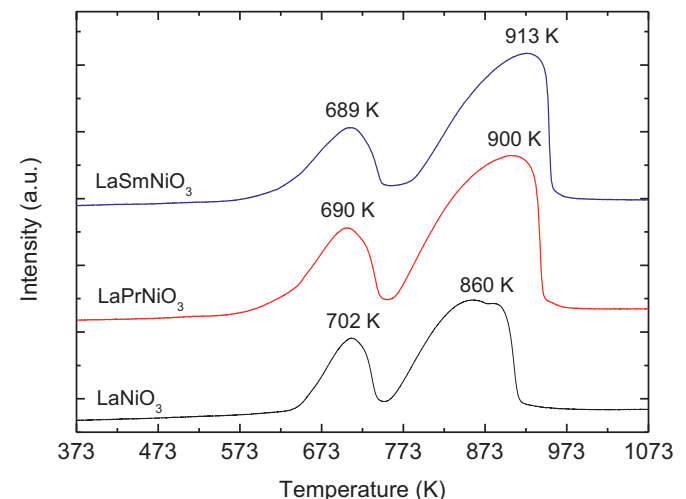


Table 1
Average sizes of Ni^0 crystallites on the reduced and passivated samples.

Sample	Size ^a (nm)
LaNiO_3	21
LaPrNiO_3	18
LaSmNiO_3	18

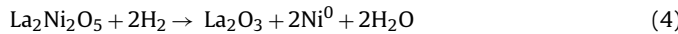
^a Determined by applying the Scherrer equation to the peak corresponding to lattice plane (111) of Ni^0 .

Fig. 3. TPR profiles of LaNiO_3 , LaPrNiO_3 and LaSmNiO_3 samples.

Table 2
H₂ consumption during TPR analyses.

Sample	Theoretical consumption ($\mu\text{mol g}_{\text{cat}}^{-1}$)	H ₂ consumed ($\mu\text{mol g}_{\text{cat}}^{-1}$) ^a	Degree of reduction (%)	(2nd PA)/(1st PA)
LaNiO ₃	6108	5940	97	2.70
LaPrNiO ₃	6103	4172	71	2.89
LaSmNiO ₃	6080	3686	65	2.90

^a Sample weight used in TPR: 50 mg.



The addition of Pr and Sm to LaNiO₃ perovskite-type oxide changed the TPR profiles. The first peak was slightly shifted to lower temperatures. This could be an indication of the incorporation of the dopants into the lattice structure of LaNiO₃ [31,32]. On the other hand, the second peaks were shifted to higher temperatures and their intensity increased. These results suggest a higher fraction of NiO segregated from the Perovskite-type structure on the substituted perovskites. De Lima et al. [37] reported the presence of three peaks in the TPR profile of LaNiO₃. The intermediate peak was attributed to the reduction of Ni²⁺ to Ni⁰ of a NiO phase. Taking into account the stoichiometry of reduction from Eqs. (3) and (4), the hydrogen consumption in the second peak should be twice of the one in the first peak, if the perovskite-type oxide is the only phase present. However, the segregation of NiO from the perovskite-type structure during calcination would lead to a higher hydrogen uptake in the second peak. The presence of Pr and Sm caused a displacement of the second peak to higher temperatures, as well as an increase in its area. These results may indicate an increase in the amount of nickel (Ni²⁺) outside the perovskite-type structure. Table 2 lists the total hydrogen uptake and the intensity ratio of the second and first reduction peaks. This ratio increased with the addition of Pr and Sm, which indicates an increase in the amount of nickel oxide segregated from the perovskite-type structure. The estimated values of the degree of reduction (D.R.) are also presented in this table. LaNiO₃ sample showed a D.R. of 97%. This result indicates that most of the nickel was incorporated into the perovskite-type structure. The D.R. was lower for doped samples, following the order: LaNiO₃ > LaPrNiO₃ > LaSmNiO₃. The decrease in D.R. for the doped samples could be associated with the increase in the amount of nickel outside the perovskite-type structure, when Pr and Sm were added. This is likely due to the stoichiometry used for the calculation of D.R. that considers the reduction of Ni³⁺ to Ni⁰. The values of D.R. should be smaller when nickel Ni²⁺ from segregated NiO phase is reduced to Ni⁰.

TPD profiles obtained for all catalysts are shown in Fig. 4. All catalysts showed similar desorption profiles and the following compounds were formed: H₂, CO, CO₂, CH₄, CH₃COCH₃, C₂H₄ and CH₃COOH. At low temperatures (300–400 K), the desorption of a small amount of acetic acid is noticed. In the temperature range of 500–700 K, it is observed two peaks for the signals corresponding to H₂, CO, CO₂, CO and CH₄ that follows identical patterns. This is likely due to the occurrence of acetic acid decomposition reaction (Eqs. (5) and (6)) [26].



It is also detected the formation of small amounts of CH₃COCH₃ and C₂H₄. These products were also observed by Basagiannis and Verykios [26]. They proposed that acetone is produced by the ketonization reaction (Eq. (7)). As far as ethylene production is concerned, the formation of a ketene (CH₂CO) intermediate was proposed according to reactions (8) and (9).

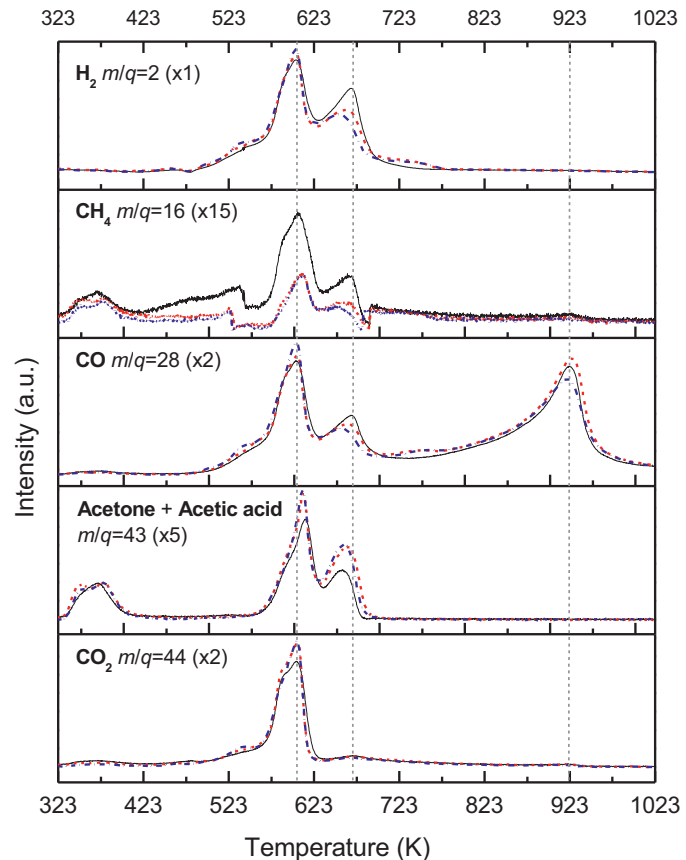


Fig. 4. TPD profiles after reduction of the samples and subsequent saturation with acetic acid. (Black solid line) LaNiO₃, (red dash line) LaPrNiO₃, (blue dash-dot line) LaSmNiO₃.



There is also a peak corresponding to the formation of CO at 900 K on the TPD profile of all catalysts. This CO is likely a reaction product of the oxidation of carbon deposited on the catalyst surface during the decomposition of acetic acid. The oxygen used for this reaction should come from the structure of La₂O₃ [37]. The presence of La leads to the formation of mixed phases with cationic vacancies which enhance the mobility of lattice oxygen anions. It may favor the surface reaction between carbon-containing species and reactive oxygen species [46].

Similar TPD profiles were reported by Basagiannis and Verykios [26] using Ni/La₂O₃/Al₂O₃ catalysts. They suggested that the TPD profiles stem from the decomposition reactions of acetic acid.

The addition of Pr and Sm did not change significantly the TPD profiles, indicating that the reaction mechanism was not altered. The only significant difference was the decrease in the intensity of the H₂ signal of LaPrNiO₃ and LaSmNiO₃ at 650 K. This result suggests that the Pr and Sm addition minimized the formation of H₂ via decomposition of acetic acid (Eq. (5)).

3.2. Catalytic tests

3.2.1. SR of acetic acid

Acetic acid conversion and product distribution as a function of time on stream (TOS) for SR of acetic acid at 873 K over LaNiO₃, LaPrNiO₃ and LaSmNiO₃ catalysts are shown in Fig. 5. The following initial conversions were observed: LaNiO₃-82%, LaSmNiO₃-98% and LaPrNiO₃-90%. The main products formed were H₂ and CO₂,

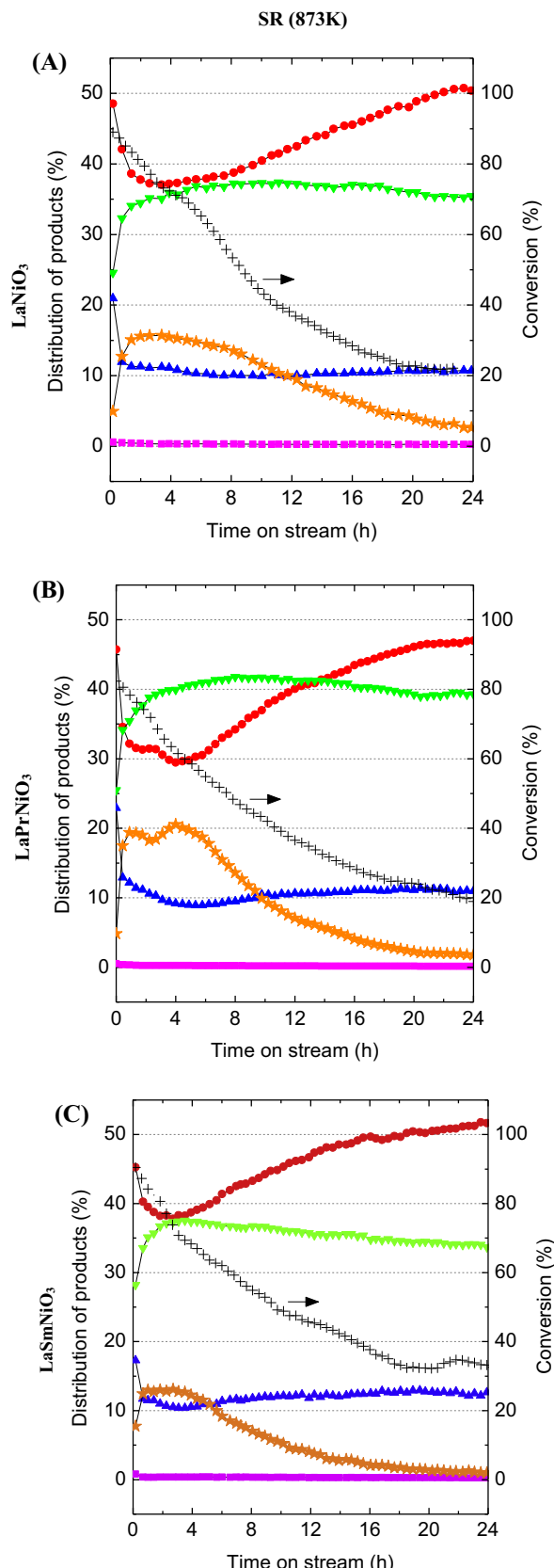


Fig. 5. Stability results at 873 K for SR on (A) LaNiO_3 , (B) LaPrNiO_3 and (C) LaSmNiO_3 catalysts. The feed is a 400 mL min^{-1} stream with 13 vol% acetic acid, 40 vol% steam and 47 vol% He ($S/\text{F}=3$). (+) Acetic acid conversion, H_2 (●), CH_4 (■), CO (▲), CO_2 (▼) and acetone (★).

Table 3
Rates of carbon accumulation under SR and OSR at 873 K.

Sample	$r_{\text{carbon}} (\text{mg}_{\text{carbon}} \text{ g}_{\text{cat}}^{-1} \text{ h}^{-1})$	
	SR (873 K)	OSR (873 K)
LaNiO_3	16.6	2.16
LaPrNiO_3	14.4	3.65
LaSmNiO_3	26.9	3.78

indicating that SR of acetic acid is the main reaction taking place. There is also the formation of small amounts of CO and acetone. These results are in agreement with the transient experiments that revealed the occurrence of acetic acid decomposition reaction (Eqs. (5) and (6)) and ketonization reaction (Eq. (7)).

3.2.2. OSR of acetic acid

Fig. 6 shows the acetic acid conversion and product distribution as a function of time on stream (TOS) for OSR of acetic acid at 873 K over LaNiO_3 , LaPrNiO_3 and LaSmNiO_3 catalysts. The initial acetic acid conversion was approximately the same for all catalysts. H_2 , CO_2 , CO and small amounts of CH_4 were formed during the OSR of acetic acid.

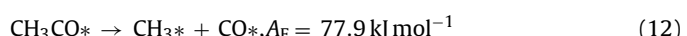
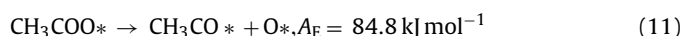
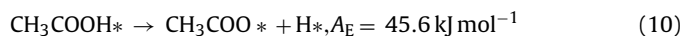
3.3. Characterization of post-reaction Ni-supported catalysts

Acetic acid conversions significantly decreased at the beginning of the SR reaction tests for all catalysts. However, the addition of oxygen to the feed significantly promoted the stability of the catalysts. In order to determine the main cause of catalyst deactivation, the used Ni-supported catalysts were characterized by TGA analysis. TPO profiles of LaNiO_3 , LaPrNiO_3 and LaSmNiO_3 catalysts after 24 h of SR and OSR at 873 K are presented in Fig. 7A and B, respectively. For SR, all catalysts showed one broad peak with maxima in the range of 879–893 K, while for OSR, the peak maximum temperatures were slightly lower, around 823–828 K.

Table 3 lists the rate of carbon accumulation on the catalyst surface after SR and OSR of acetic acid for 24 h TOS. For SR of acetic acid, the amount of carbon formed followed the order: $\text{LaPrNiO}_3 < \text{LaNiO}_3 < \text{LaSmNiO}_3$.

4. Discussion

In the present work, the catalytic activities and selectivities of LaNiO_3 , LaPrNiO_3 and LaSmNiO_3 catalysts have been investigated in the SR and OSR reactions. The product distribution was quite similar for all catalysts, as it was previously observed in the transient experiments. Wang et al. [18] studied the steam reforming of acetic acid (SR) using theoretical (DFT, density functional theory) calculations and proposed the reaction pathway described by Eqs. (10)–(13). According to the authors, the initial decomposition of acetic acid on the surface of Co-based catalysts may take two distinct routes. In the first route, acetic acid is adsorbed with abstraction of an H atom and converted into adsorbed acetate species (CH_3COO^*) (Eq. (10)). Once formed the acetate species is easily decomposed into acetyl species (CH_3CO^*) (Eq. (11)), which decomposes into CH_3^* and CO^* radicals (Eq. (12)). The radical CO^* is oxidized or desorbed but the radical CH_3^* may take two different pathways: (i) it is hydrogenated to CH_4 or (ii) it undergoes successive dehydrogenation and forms carbon (C^*) [19,20]. The deposited carbon is than oxidized with O^* atoms provided by water, cleaning the catalyst surface (Eq. (13)).



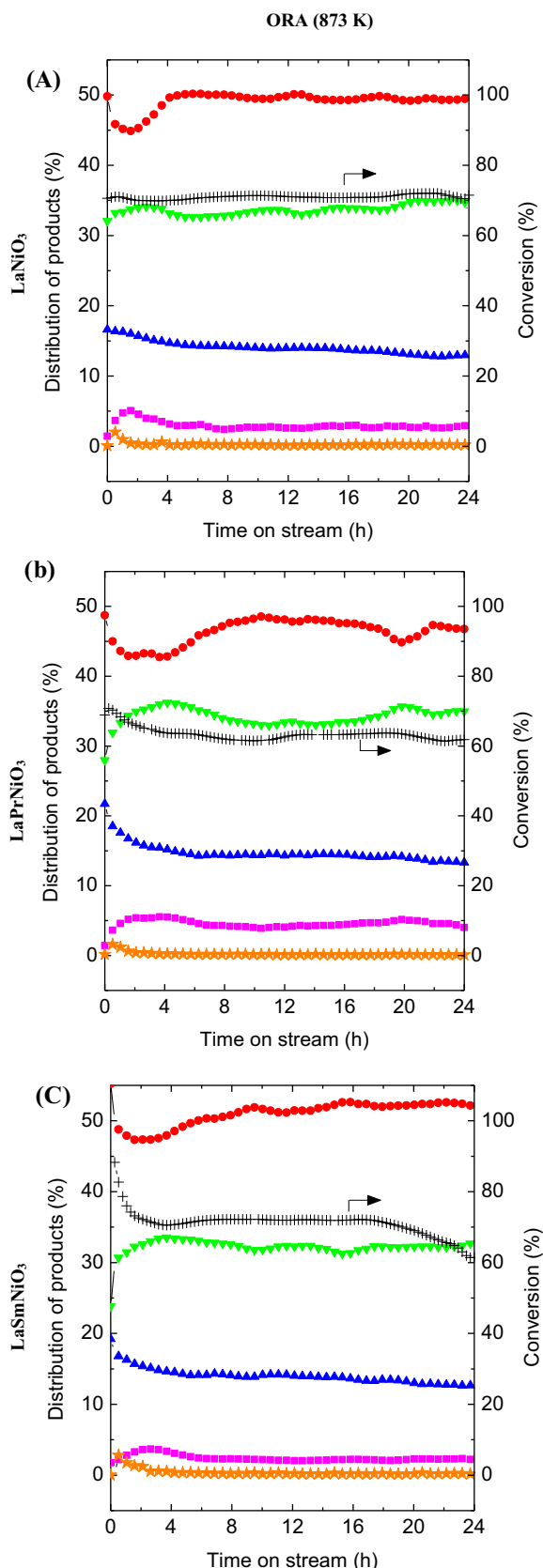


Fig. 6. Stability results at 873 K for OSR on (A) LaNiO_3 , (B) LaPrNiO_3 and (C) LaSmNiO_3 catalysts. OSR conditions: 205 mL min^{-1} stream with 11 vol% acetic acid, 13 vol% steam, 2 vol% O_2 and 74 vol% Ar ($\text{S:F:O}_2 = 1.08:1:0.18$). (+) Acetic acid conversion, H_2 (●), CH_4 (■), CO (▲), CO_2 (▽) and acetone (★).

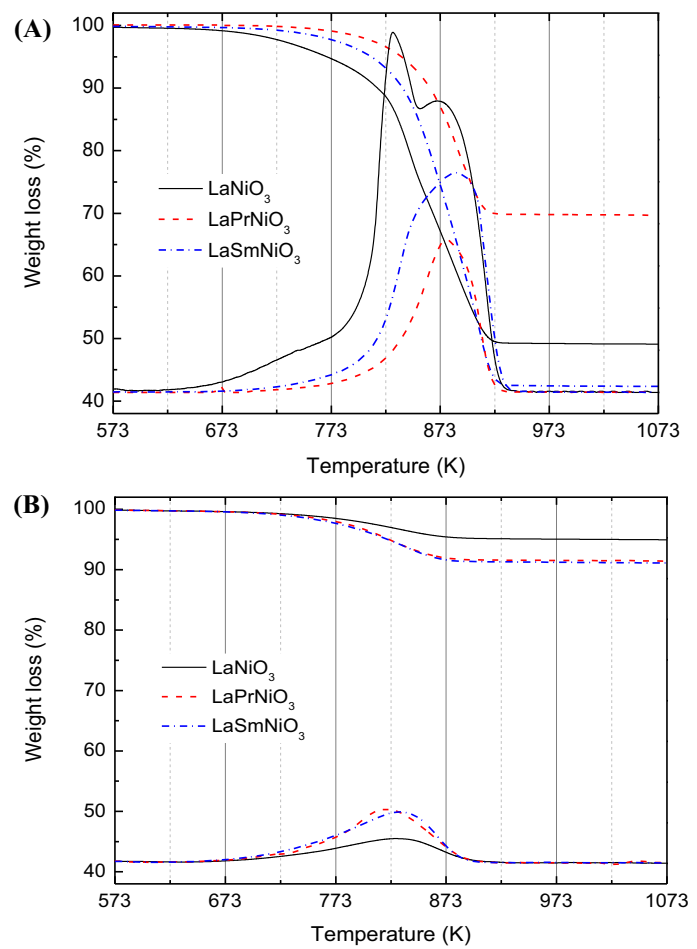
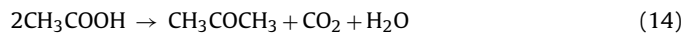


Fig. 7. TGA profiles of LaNiO_3 , LaPrNiO_3 and LaSmNiO_3 samples.

In the SR, the selectivity to H_2 and CO decreases, whereas the formation of acetone and CO_2 increases in the first 2 h with TOS. Then, the selectivity to H_2 and CO continuously increased, while the production of CO and acetone decreased. After 18 h TOS, acetone is no longer detected for LaPrNiO_3 and LaSmNiO_3 catalysts. Ketonization is an alternative route in the conversion of acetic acid over polycrystalline oxide samples [17]. It is a bimolecular reaction in which two molecules of acetic acid are coupled to produce the symmetric ketone (in this case, acetone), also generating water and CO_2 as byproducts (Eq. (14)).



Basagiannis and Verykios [26] carried out the TPD of acetic acid over Al_2O_3 , La_2O_3 and $\text{Ni/La}_2\text{O}_3/\text{Al}_2\text{O}_3$. Ketonization reaction with the formation of acetone and CO_2 occurred over both supports. However, this reaction did not take place over the catalyst. According to the authors, metallic nickel promotes the decomposition reaction of acetic acid. In the present work, the increasing formation of acetone and CO_2 is likely due to the oxidation of the metallic Ni particles by the water in the feed. Then, the NiO particles formed were reduced again to metallic Ni particles by the syngas produced during the SR reforming reaction. The formation of metallic Ni particles that are the active sites for the SR of acetic acid led to an increase in the selectivity to H_2 and CO and the disappearance of acetone. The selectivity to CO_2 did not decrease significantly likely due to the occurrence of water gas-shift reaction, which produces CO_2 at the expense of CO selectivity decrease. The reduction of the NiO particles formed during reaction seems to be more effective for the doped catalysts. The oxidation of the metallic particles by

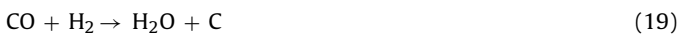
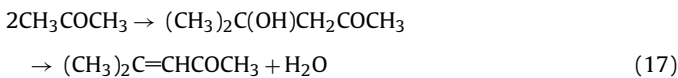
the feed has also been reported for the SR of ethanol over Ni- or Co-supported catalysts [20]. The absence of methane is associated with the activity of Ni particles for SR under this reaction conditions.

On the contrary to SR, in the OSR the acetone was formed only in trace amounts, indicating that ketonization reaction did not occur for OSR. Kugai et al. [47] reported that the addition of water and oxygen promotes C–C bond cleaving, which can explain the decrease in acetone formation during OSR in comparison with SR [37]. The addition of O₂ to the feed also improved catalyst stability. In the SR, the conversions decrease during the reaction time for all samples, while the SRO conversions were stable. De Lima et al. [37] also observed that the use of a small oxygen amount increased the stability of LaNiO₃ in the oxidative steam reforming of ethanol. These authors showed that in the presence of oxygen, carbon formation was significantly decreased, which resulted in enhanced stability. Furthermore, the addition of oxygen to the feed increased the selectivity to CO and decreased the formation of CO₂. This result is also related to the inhibition of ketonization rate reaction, which contributes to decrease the formation of CO₂. Medrano et al. [48] also noted the decrease in the CO₂ yields during the SRO of acetic acid, with the correspondent decrease in CO formation. According to them, the partial oxidation of acetic acid (Eq. (15)) is taking place in the presence of oxygen. They also reported a decrease in the H₂ yield when the percentage of oxygen addition increases. In this work, the decrease in the H₂ yield was not observed, probably because of the small O₂ concentration used.



The different peaks observed in the TPO profiles of the catalysts used in the SR can be associated with different types of carbon formed during the reaction such as amorphous carbon, filamentous carbon and graphitic carbon. The oxidation peak located below 673 K is ascribed to amorphous carbon, whereas the peak above 773 K corresponds to carbon nanotubes. The oxidation of graphite occurs at higher temperatures (973 K) [49]. Basagiannis and Verykios [26] reported a TPO profile of Ni/La₂O₃/Al₂O₃ catalyst after SR of acetic acid at 773 or 973 K, which revealed the presence of two peaks. The low-temperature oxidation peak (623 K) was attributed to the carbon deposited on the surface of metallic particles. The peak at high temperature (923 K) was due to the oxidation of carbon filaments. Therefore, in this work, the TPO profiles indicate the formation of carbon filaments during SR and OSR of acetic acid for all catalysts. The addition of oxygen to the feed in the OSR significantly decreased the amount of carbon deposited over all catalysts. Oxygen from the feed enhances the gasification rate of the carbon deposits formed, which improves catalyst stability. In this case, the amount of carbon formed over all catalysts was approximately the same.

The main reactions that may contribute to coke formation during acetic acid conversion reactions are as follows [50]: (i) ethylene formation, followed by polymerization to coke (Eq. (16)); (ii) ketonization reaction followed by dehydration to mesityl oxide (MO) (Eq. (17)); (iii) the Boudouard reaction (Eq. (18)); (iv) the reverse of carbon gasification (Eq. (19)); and (v) the decomposition of hydrocarbons such as methane (Eq. (20)) and ethylene.



The extent of each reaction depends on both reaction conditions and the catalyst used [22,50]. While low reaction temperatures favor the formation of carbon through reactions (18) and (19), carbon formation via reactions (19) and (20) are the main routes at higher temperatures. The removal of carbon deposits from the surface can be represented by Eq. (13).

According to Gallego et al. [35], praseodymium oxide (Pr₂O₃) has redox properties, which may explain the lower rate of carbon accumulation in the sample LaPrNiO₃. Praseodymium oxide can promote the cleaning of the catalyst surface according to Eq. (21).



The acid/base properties of the support, which exhibits activity for this reaction, also determine the reaction pathways and, as a consequence, also influence catalyst stability. The support can play a major role in the acetic acid conversion reactions by assisting in the removal of carbon or suppressing its formation.

In our work, the TPR profiles are in agreement with the in situ XRD data (Fig. 2). These analyses showed that the perovskite phases LaNiO₃ and La₄Ni₃O₁₀ were destroyed after reduced producing metallic Ni particles deposited over La₂O₃. Fatsikostas et al. [27] proposed that the La₂O₃ could react with CO₂ to produce La₂O₂CO₃ (Eq. (22)). This lanthanum oxycarbonates can react with carbon deposited to form CO and regenerate La₂O₃ by promoting the removal of carbon (Eq. (23)).



The partial substitution of La by Pr decreased the amount of carbon formed. According to Gallego et al. [35], the sample derived from LaPrNiO₃ presents redox properties, which are related to the presence of praseodymium oxide (Pr₂O₃). This could explain the lower coke deposition observed for this sample. Pr₂O₃ can promote the cleaning of the surface of the catalyst following equation.



5. Conclusions

The data show that the precipitation method was effective to form the perovskite-type structure. All samples showed good reducibility and the addition of dopants (Pr and Sm) changed slightly the reduction profiles. This structure is destroyed during the reduction process, giving rise to Ni⁰ particles dispersed over La₂O₃. The presence of La₄Ni₃O₁₀ had no effect on the properties of the catalyst formed after reduction. This can be confirmed by the XRD of the passivated samples and by the in situ XRD analysis. The presence of dopants did not alter significantly the XRD patterns of the precursors nor the average crystallite sizes. Data from steam reforming of acetic acid showed that the perovskite-type are selective catalytic precursors for hydrogen production. This high selectivity may be explained by the fact that the surface of these samples adsorb and decompose the acetic acid as observed in TPD analysis. The values of selectivity for the three precursors studied during the reaction of steam reforming were very similar. Thus, it can be affirmed that the changes obtained by doping the LaNiO₃ structure with Pr or Sm did not alter significantly the catalytic performance of these materials. TGA analysis showed that the catalyst doped with Pr had the lowest accumulation of coke, probably due to the redox properties of this metal. The catalytic oxidative reforming tests showed that the presence of a small amount of O₂ contributes to reduce the formation of coke which helps the catalyst does not deactivate during the reaction. Among the conditions studied, the best selectivity for hydrogen was

obtained at 873 K with a little amount of O₂. It was concluded that among the precursors studied, LaNiO₃ showed the best cost benefit. The addition of Pr and Sm in the crystal structure of perovskite-type increased the cost of the catalyst, without significantly affecting the catalytic.

Acknowledgments

The authors wish to acknowledge the financial support provided CAPES, FAPEMIG, CNPq, and Vale S.A. The authors are also grateful to the Brazilian Synchrotron Light Laboratory (LNLS) for providing facilities and technical support at the D10B-XPD beamline.

References

- [1] S.A. Chattanathan, S. Adhikari, N. Abdoulmoumine, *Renew. Sustain. Energ. Rev.* 16 (2012) 2366–2372.
- [2] A. Tanksale, J.N. Beltramini, G.M. Lu, *Renew. Sustain. Energ. Rev.* 14 (2010) 166–182.
- [3] G.W. Huber, J.A. Dumesic, *Catal. Today* 111 (2006) 119–132.
- [4] E.C. Vagia, A.A. Lemonidou, *Appl. Catal. A: Gen.* 351 (2008) 111.
- [5] N. Iwasa, T. Yamane, M. Takei, J. Ozaki, M. Arai, *Int. J. Hydrogen Energy* 35 (2010) 110–117.
- [6] M. Garcia-Perez, A. Chaala, H. Pakdel, D. Kretschmer, C. Roy, *Biomass Bioenergy* 31 (2007) 222–242.
- [7] D. Mohan, Pittman F.C.U. Jr., P.H. Steele, *Energy Fuels* 20 (2006) 848–889.
- [8] Z. Luo, S. Wang, Y. Liao, J. Zhou, Y. Gu, K. Cen, *Biomass Bioenergy* 26 (2004) 455–462.
- [9] J.A. Medrano, M. Oliva, J. Ruiz, L. García, J. Araizo, *Energy* 36 (2011) 2215–2224.
- [10] C. Yan, F. Cheng, R. Hu, *Int. J. Hydrogen Energy* 35 (2010) 11693–11699.
- [11] R. Trane, S. Dahl, M.S. Skjøth-Rasmussen, A.D. Jensen, *Int. J. Hydrogen Energy* 37 (2012) 6447–6472.
- [12] D. Wang, S. Czernik, E. Chorne, *Energy Fuels* 12 (1998) 19–24.
- [13] L. García, R. French, S. Czernik, E. Chornet, *Appl. Catal. A: Gen.* 201 (2000) 225–239.
- [14] X. Hu, G. Lu, *J. Mol. Catal. A: Chem.* 261 (2007) 43–48.
- [15] M.C. Ramos, A.I. Navascués, L. García, R. Bilbao, *Ind. Eng. Chem. Res.* 46 (2007) 2399–2406.
- [16] E.C. Vagia, A.A. Lemonidou, *Int. J. Hydrogen Energy* 32 (2007) 212–223.
- [17] R. Martinez, M.C. Huff, M.A. Barreau, *J. Catal.* 222 (2004) 404–409.
- [18] S. Wang, X. Li, L. Guo, Z. Luo, *Int. J. Hydrogen Energy* 37 (2012) 11122–11131.
- [19] C.N. Ávila-Neto, J.W.C. Liberatori, A.M. da Silva, D. Zanchet, C.E. Hori, F.B. Noronha, J.M.C. Bueno, *J. Catal.* 287 (2012) 124–137.
- [20] C.N. Ávila-Neto, D. Zanchet, C.E. Hori, R.U. Ribeiro, J.M.C. Bueno, *J. Catal.* 307 (2013) 222–237.
- [21] S.C. Dantas, K.A. Resende, R.L. Rossi, A.J. Assis, C.E. Hori, *Chem. Eng. J.* 197 (2012) 407–413.
- [22] Z. Li, X. Hu, L. Zhang, S. Liu, G. Lu, *Appl. Catal. A: Gen.* 417–418 (2012) 281–289.
- [23] J.A. Medrano, M. Oliva, J. Ruiz, L. García, J. Arauzo, *J. Anal. Appl. Pyrol.* 85 (2009) 214–225.
- [24] X. Hu, G. Lu, *Appl. Catal. B: Environ.* 99 (2010) 289–297.
- [25] S. Thaicharoenutcharittham, V. Meeyoo, B. Kitayanan, P. Rangsuvigit, T. Rirk-somboon, *Catal. Today* 164 (2011) 257–261.
- [26] A.C. Basagiannis, X.E. Verykios, *Appl. Catal. A: Gen.* 308 (2006) 182–193.
- [27] A.N. Fatsikostas, D.I. Kondarides, X.E. Verykios, *Catal. Today* 75 (2002) 145–155.
- [28] D.L. Trimm, *Catal. Today* 49 (1999) 3–10.
- [29] R. Pereñíguez, V.M. González-DelaCruz, J.P. Holgado, A. Caballero, *Appl. Catal. B: Environ.* 93 (2010) 346–353.
- [30] G. Pecchi, P. Reyes, R. Zamora, C. Campos, L.E. Cadús, B.P. Barbero, *Catal. Today* 133 (2008) 420–427.
- [31] S.O. Choi, S.H. Moon, *Catal. Today* 146 (2009) 148–153.
- [32] A.K. Norman, M.A. Morris, *J. Mater. Process. Technol.* 92 (1999) 91–96.
- [33] Z. Zhang, M. Greenblatt, *J. Solid State Chem.* 117 (1995) 236–246.
- [34] J.L.G. Fierro, J.M.D. Tascón, L.G. Tejuca, *J. Catal.* 93 (1985) 83–91.
- [35] G.S. Gallego, J.G. Marín, C. Batiot-Dupeyrat, J. Barrault, F. Mondragón, *Appl. Catal. A: Gen.* 369 (2009) 97–103.
- [36] A. Jahangiri, H. Pahlavanzadeh, H. Aghabozorg, *Int. J. Hydrogen Energy* 37 (2012) 9977–9984.
- [37] S.M. de Lima, A.M. da Silva, L.O.O. da Costa, J.M. Assaf, G. Jacobs, B.H. Davis, L.V. Mattos, F.B. Noronha, *Appl. Catal. A: Gen.* 377 (2010) 181–190.
- [38] J.L. García-Muñoz, J. Rodríguez-Carvajal, P. Lacorre, J.B. Torrance, *Phys. Rev. B* 46 (1992) 4414–4425.
- [39] P. Gordes, N. Christiansen, E.J. Jensen, J. Villadsen, *J. Mater. Sci.* 30 (1995) 1053–1058.
- [40] S.M. de Lima, A.M. da Silva, L.O.O. da Costa, J.M. Assaf, L.V. Mattos, R. Sarkari, A. Venugopal, F.B. Noronha, *Appl. Catal. B: Environ.* 121 (2012) 1–9.
- [41] H. Li, Q. Liang, L.Z. Gao, S.H. Tang, Z.Y. Cheng, B.L. Zhang, Z.L. Yu, C.F. Ng, C.T. Au, *Chin. Chem. Lett.* 12 (2001) 839–842.
- [42] R. Pereñíguez, V.M. González-delaCruz, A. Caballero, J.P. Holgado, *Appl. Catal. B: Environ.* 123–124 (2012) 324–332.
- [43] D.G. Mustard, C.H. Bartholomew, *J. Catal.* 67 (1981) 186–206.
- [44] M.E. Rivas, C.E. Hori, J.L.G. Fierro, M.R. Goldwasser, A. Griboval-Constant, 184, *Journal of Power Sources* (2008) 265–275.
- [45] M. Crespin, P. Levitz, L. Gatinea, *J. Chem. Soc. Faraday Trans 2* (1983) 1181–1194.
- [46] U. Olsbye, O. Moen, A. Slagtern, I.M. Dahl, *Appl. Catal. A: Gen.* 228 (2002) 289–303.
- [47] J. Kugai, S. Velu, C. Song, *Catal. Lett.* 101 (2005) 255–264.
- [48] J.A. Medrano, M. Oliva, J. Ruiz, L. García, J. Arauzo, *Int. J. Hydrogen Energy* 33 (2008) 4387–4396.
- [49] B. Kitayanan, W.E. Alvarez, J.H. Harwell, D.E. Resasco, *Chem. Phys. Lett.* 317 (2000) 497–503.
- [50] L.V. Mattos, G. Jacobs, B.H. Davis, F.B. Noronha, *Chem. Rev.* 112 (2012) 4094–4123.